Mon. Not. R. Astron. Soc. **000**, 1–18 (2009) Printed 12 March 2010 (MN LATEX style file v2.2)

Small-spatial scale variations of nebular properties and the abundance discrepancy in three Galactic H II regions⋆

A. Mesa-Delgado† and C. Esteban
Instituto de Astrofísica de Canarias, E-38200 La Laguna, Tenerife, Spain
Departamento de Astrofísica, Universidad de La Laguna, E-38205 La Laguna, Tenerife, Spain

Accepted 2010 March 8. Received 2010 March 1; in original form 2009 December 14.

ABSTRACT
We present results of long-slit spectroscopy in several slit positions that cover different morphological structures of the central parts of three bright Galactic H II regions: M8, M17 and NGC 7635. We study the spatial distributions of a large number of nebular parameters such as the extinction coefficient, line fluxes, physical conditions and ionic abundances at the maximum spatial resolution attainable with our instrumentation. Particularly, our goal is to study the behaviour of the abundance discrepancy factor of O^{2+}, ADF(O^{2+}), defined as the logarithmic difference of the O^{2+} abundances derived from collisionally excited and recombination lines. We find that the ADF(O^{2+}) remains fairly constant along the slit positions of M8 and M17. In the case of NGC 7635, we only detect the O II recombination lines in the integrated spectrum along the whole slit, where the ADF(O^{2+}) reaches a remarkably high value of about 0.59 dex. We compare our results with previous ones obtained for the Orion Nebula. We find several evidences that suggest the presence of a candidate to Herbig-Haro object in M8.

Key words: H II regions – ISM: abundances – ISM: individual: M8 – ISM: individual: M17 – ISM: individual: NGC 7635

1 INTRODUCTION

The study of the elemental abundances in H II regions is an essential tool for our knowledge of the chemical evolution of the universe. Traditionally, ionic abundances relative of the elements heavier than He have been determined from the strong collisionally excited lines (CELs). More than 20 years ago, French (1983) obtained the first determination of the C^{2+}/H^+ ratio derived from the faint recombination line (RL) C II 4267 Å for a planetary nebula (PN), finding that it was several orders of magnitude larger than the abundance obtained from the CELs of this ion. Later, this result was confirmed in other PNe (*e.g.* Rola & Stasinska 1994; Mathis & Liu 1999). A similar qualitative result was also found by Peimbert et al. (1993) for the O^{2+}/H^+ ratio in the Orion Nebula: the abundances obtained from the flux of the faint RLs were higher than those derived using the standard method based on CELs. Currently, this observational fact is a classical problem in the understanding of the physics of photoionized nebulae known as "Abundance Discrepancy" (AD) problem. This disagreement is quantified by means of the Abundance Discrepancy Factor (ADF) that can be defined as the ratio, or the logarithmic difference, between abundances of a same ion derived from RLs and CELs. In the case of the O^{2+}/H^+ ratio, the ADF has rather similar values between 0.1 and 0.3 dex for extragalactic and Galactic H II regions (*e.g.* García-Rojas et al. 2005; García-Rojas & Esteban 2007; Esteban et al. 2009), while for PNe the ADF shows a much wider range of values, becoming substantially larger in some object (*e.g.* Liu et al. 2000, 2006; Tsamis et al. 2004, 2008).

What causes the AD problem is nowadays debated. On the one hand, the predictions of the temperature fluctuations paradigm proposed by Peimbert (1967), and characterized by the mean square of the spatial distribution of temperature –the so-called temperature fluctuations parameter, t^2– seems to explain the ADF observed in H II regions, as it is argued by García-Rojas & Esteban (2007). Under this scheme, the AD problem is a direct consequence of the different temperature dependence of the emissivities of the lines used: in the case of CELs, it depends exponentially on the electron temperature, T_e, of the ionized gas, while the emissivity of RLs has a power law temperature dependence, similar to those of the Balmer lines used as reference to determine the ionic abundance ratio relative to H^+. On the other

⋆ Based on observations made with the 4.2m William Herschel Telescope (WHT) operated on the island of La Palma by the Isaac Newton Group in the Spanish Observatorio del Roque de los Muchachos of the Instituto de Astrofísica de Canarias.
† E-mail: amd@iac.es

hand, the hypothesis suggested by Liu et al. (2000), where most of the emission of RLs come from a cold hydrogen-poor component immersed in the ambient gas which emits the bulk of CELs, seems to solve the AD problem in PNe with high ADF values. This hypothesis is based on the observed fact that certain PNe contain well resolved H-deficient knots which are strong metallic RL emitters (*e.g.* Abell 30, Harrington & Feibelman 1984).

The existence and origin of the temperature fluctuations is controversial because high values of the t^2 parameter are not reproduced by standard photoionization models (Kingdon & Ferland 1995; Rodríguez & García-Rojas 2010) and additional mechanisms are proposed in order to explain the presence of temperature fluctuations (see revisions of Esteban 2002; Peimbert & Peimbert 2006). In the same way, new scenarios try to find a solution to the AD problem in H II regions putting forward new physical mechanisms. This is the case of the hypothesis presented by Tsamis & Péquignot (2005) and Stasińska et al. (2007). Based on the chemical model for the heavy-elements mixing of Tenorio-Tagle (1996), these authors proposed the presence of two components of different chemical composition and physical conditions in H II regions. The component responsible of most of the emission of RLs consists of cold metal-rich droplets from supernova ejecta still not mixed with the ambient gas of the H II region where most of the CEL emission would be produced. Then, note that assuming a chemically inhomogeneous model in H II regions in order to explain the AD problem, the abundance derived from RLs and CELs would be upper and lower limits, respectively, of the real abundance of the ionized gas (Stasińska et al. 2007). Recently, a new scenario have been proposed by Ercolano (2009) based on the existence of high-density quasi-neutral clumps –embedded in the nebular gas ionized by the extreme-ultraviolet (EUV) radiation– which are ionized mainly by the X-ray emission from the central star. Under this scheme, the CEL emission mainly comes from the region ionized by the EUV radiation (E region), while the RLs are emitted in different proportions from the clumps (X region) and the E region. In this sense, the abundances of the E region would be representative of the nebula and those from CELs would be easier to correct than RL ones. Contrary to the model proposed by Tsamis & Péquignot (2005) and Stasińska et al. (2007), the nebular model of Ercolano (2009) has homogeneous abundances.

In a previous paper (Mesa-Delgado et al. 2008) we explored the behaviour of the AD at small spatial scales and its dependence on different nebular parameters and physical conditions in the Orion Nebula in order to shed light on the origin of the AD problem. In that study, we used long-slit spectroscopy at spatial scales of $1\farcs2$, finding high ADF(O^{2+}) values related to the presence of Herbig-Haro (HH) objects and temperature spikes at the position of the protoplanetary discs (proplyds). A subsequent detailed analysis of HH 202 was carried out by Mesa-Delgado et al. (2009) using integral field spectroscopy confirming a high ADF(O^{2+}) value at the main knot of HH 202 in agreement with the results of Mesa-Delgado et al. (2008). Another important result of Mesa-Delgado et al. (2009) was the obtention –for the first time in an H II region– of a map of the Balmer temperature and of the temperature fluctuations in the observed field, finding no correlation between the ADF(O^{2+}) and the t^2 parameter.

Following the same goals and methodology of Mesa-Delgado et al. (2008), in this paper we have used long-slit spectroscopy at intermediate spectral resolution in order to study the spatial distribution of the ADF(O^{2+}) and other main nebular properties as well as their relation with the local morphological structures (*e.g.* density condensations, ionization fronts or HH objects) in other bright Galactic H II regions, namely, M8, M17 and NGC 7635.

After the Orion Nebula, M8 and M17 are probably the most studied Galactic H II regions. M8 forms a blister of photoionized material on the surface of a giant molecular cloud. Near the optical center the region with the highest surface brightness of the nebula is found, the Hourglass (HG) region. This region is mainly ionized by the O star Herschel 36 (Her 36), while the stars HD 165052 and 9 Sgr ionize the rest of the nebula (Woodward et al. 1986). M17 is a cavity with a V shape and the V opening in the line of sight. The main ionization source of M17 is a group of O3-O4 stars, which belong to the open cluster NGC 6618, located in the dark bay of the nebula (Hanson & Conti 1995). A singular characteristic of M17 is its rather high ionization degree –O^{2+}/O^{+} ratio– in comparasion with other Galactic H II regions. The chemical composition of M8 and M17 have been widely studied by several authors in all spectral ranges from low to high spectral resolution (*e.g.* Rubin 1969; Peimbert & Costero 1969; Sánchez & Peimbert 1991; Rodríguez 1999; Esteban et al. 1998; Tsamis et al. 2003). Based on high resolution and deep echelle spectrophotometry, García-Rojas et al. (2007) have provided a complete revision of the chemical abundances of these H II regions using CELs and RLs. Nevertheless, we have not found in the literature detailed studies about the spatial behaviour of the nebular properties of these regions, excluding that of Peimbert et al. (1992) along of 17 areas of M17 at low spectral resolution. Our third region, NGC 7635, is not a classical H II region. This nebula is an interstellar bubble formed by the interaction of the stellar wind of the O6.5 IIIf star BD+60 2522 with the surrounding interstellar medium. Recently works assume that the ram pressure of the stellar wind is balanced by the surrounding gas pressure due to the similarity between the velocities of the the molecular cloud and the bright nebulosity places of the nebula (Christopoulou et al. 1995; Moore et al. 2002). The study of physical conditions and chemical abundances in NGC 7635 have been restricted to some selected zones (Talent & Dufour 1979; Rodríguez 1999; Moore et al. 2002). Moore et al. (2002) have been the first in exploring the spatial distributions of several bright emission lines –[O III] 5007 Å, Hα and [N II] 6584 Å– along the set of knots located at northwest of the central star and the rim of the bubble. These authors also obtained the first density spatial profile along the slit position that covered the knots.

In Section 2 we describe the observations of the Galactic H II regions, the reduction procedure and the extraction of the one-dimensional spectra. In Section 3 we enumerate the selected emission lines and describe the procedure used to measure the fluxes and the extinction correction applied for each nebula. In Section 4 we describe the method used to determine the physical conditions and the ionic abundances from both kinds of lines, CELs and RLs. In Section 5 we present and discuss the spatial distributions along the

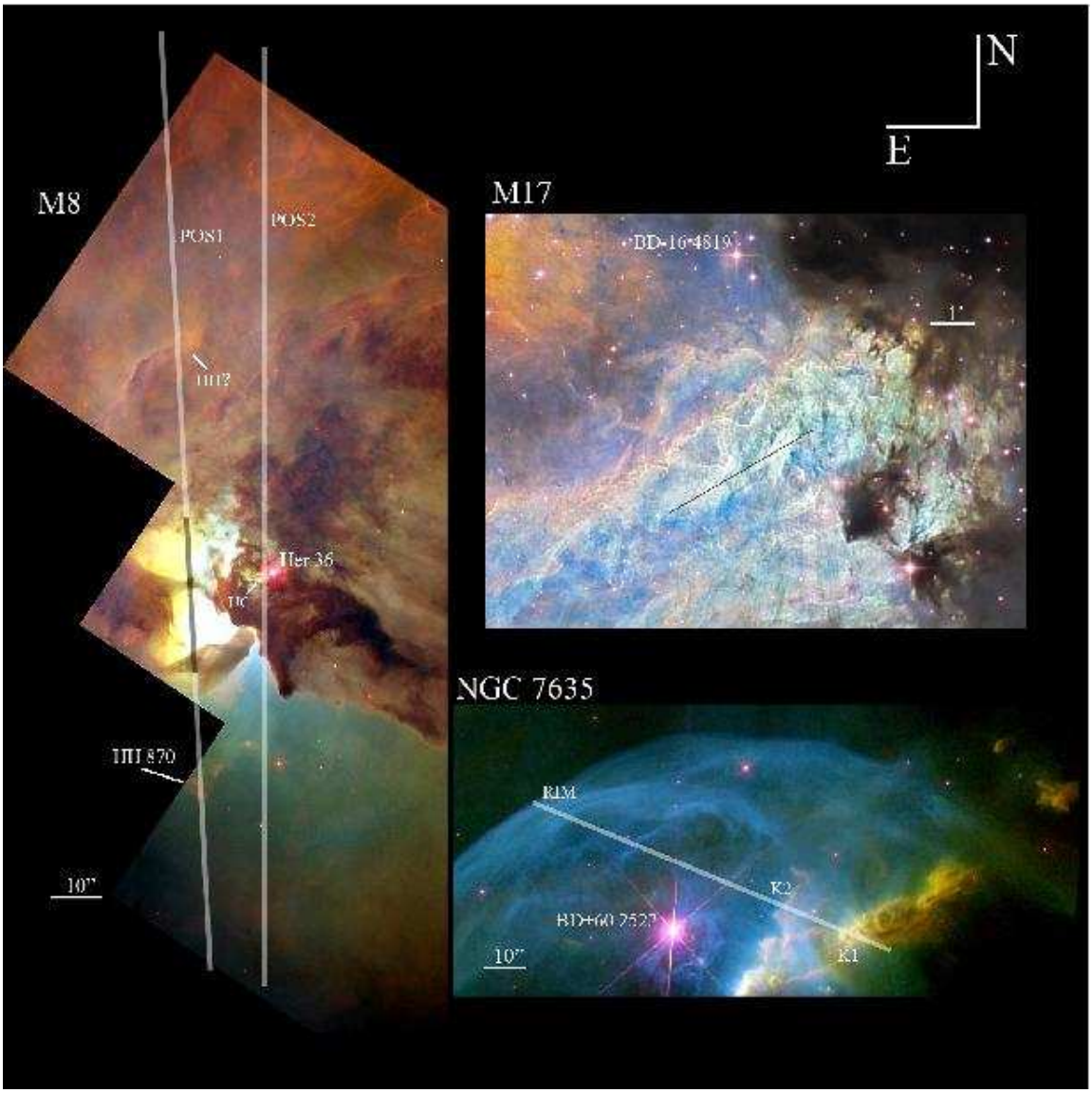

Figure 1. Observed slit positions over the central parts of the three Galactic H II regions. The slits only show the total extraction area, while the total slit length is 3.′8. The positions of the candidates to proplyd (Stecklum et al. 1998) and HH object (see §7.3) are indicated as UC and HH?, respectively. The images are combinations of exposures taken with different narrow-band filters. For all regions, emission from [O III] is shown in blue, emission from Hα is shown in green and emission from [S II] is shown in red. M8 and NGC 7635 images are sections of combinations of WFPC2 images –Caulet (1997) and Moore et al. (2002), respectively. The M17 image is a section of the original mosaic obtained by the amateur astronomer I. de la Cueva Torregrosa.

slit positions of several nebular quantities for each nebula. In Section 6 we show the physical conditions and the ionic abundances for the individual extractions of NGC 7635 as well as discuss the puzzling abundance pattern found in this object. In Section 7 we compare the results on the light of the different lineal spatial resolution attained in this paper with that of the observations of Mesa-Delgado et al. (2008) in the case of the Orion Nebula. We also present several arguments for the presence of a new HH object in M8 and discuss the possible causes of the high ADF(O^{2+}) found in NGC 7635. Finally, in Section 8 we summarize the main conclusions of the paper.

2 OBSERVATIONS, DATA REDUCTION AND EXTRACTION OF THE ONE-DIMENSIONAL SPECTRA

Long-slit spectra at intermediate spectral resolution were obtained on 18 July 2007 and 11 May 2008 using the Intermediate dispersion Spectrograph and Imaging System (ISIS) at the 4.2m William Herschel Telescope (WHT) in the Observatorio del Roque de los Muchachos (La Palma, Spain). Two different CCDs were used at the blue and red arms of the spectrograph: an EEV12 CCD with a configuration 4096×2048 pixels with a size of 13.5μm per pixel in the blue arm and a REDPLUS CCD with 4096×2048 pixels with a pixel size of 15μm in the red arm. The spatial scale was 0.″20 pixel^{-1} and 0.″22 pixel^{-1} in the blue and red arm, respec-

tively. The slit length was 3′.8 and the slit width was fixed to 0″.98. The R1200B grating was used in the blue arm and the R316R one in the red arm. These gratings gave an effective spectral resolution of 0.86 and 3.81 Å for the blue and red arms, respectively. The blue spectra covered the spectral range from 4220 to 5080 Å and the red one from 5320 to 8100 Å. The observation nights were photometric and the seeing during both observations was between of 0″.5 and 0″.8.

The Galactic H II region M8 and the wind-blown nebula NGC 7635 were observed on 18 July 2007. In the case of M8, we observed two slit positions (POS1 and POS2) centered at the HG region with different position angles (see Fig. 1, the HG region is indicated by a grey section over the slit of POS1). These positions were chosen in order to cover different morphological structures such as a candidate to proplyd (Stecklum et al. 1998) marked as UC in Fig. 1 and the prominent HH 870. Unfortunately, during the analysis of these data, we noticed that probably the proplyd was not covered by the slit as we expected due to the difficulty of positioning the slit so close to the bright star Her 36. In the case of NGC 7635, a single slit position was used to cover the bright knots K1 and K2 as well as the rim of the bubble (see Fig. 1). On 11 May 2008 a single slit position was observed over the Galactic H II region M17 covering a high surface brightness zone. For all objects, large and short exposures were taken at each slit position and spectral range in order to achieve a good signal-to-noise ratio in the faint C II and O II RLs and to avoid saturation of the brightest emission lines. The journal of observations can be found in Table 1 where we present the coordinates (RA, DEC) and the position angle (PA) of each slit position observed as well as the total exposure times.

All CCD frames were reduced using the standard IRAF[1] TWODSPEC reduction package to perform bias correction, flat-fielding, cosmic-ray rejection, wavelength and flux calibration. The wavelength calibration was carried out with a CuNe+CuAr lamp. The absolute flux calibration was achieved by observations of the standard stars BD+33 2642, BD+28 4211 and BD+25 4655 for the first night and BD+25 3941, Feige 34 and BD+33 2642 for the second one. The error of the flux calibration is of the order of 5 per cent.

The extraction of the one-dimensional spectra was done using an IRAF script based on APALL task, following the procedure explained in Mesa-Delgado et al. (2008). We extracted the apertures for each region applying the bidimensional fit to the spectra of a standard star (with positional coordinates more similars to the object) used for flux calibration on the bidimensional image. In all cases, we adjusted a third-order Chebyshev polynomial obtaining a typical *rms* between 0.05 and 0.08 pixels. The slit center in the red arm was some pixels displaced with respect to the slit center in the blue arm; this effect was also corrected in the extraction procedure, and later verified from the alignment of Hα and Hβ spatial profiles, ensuring the same spatial coverage in both ranges. We also discarded apertures located at the edges of the CCD.

[1] IRAF is distributed by National Optical Astronomical Observatories, operated by the Associated Universities for Research in Astronomy, under cooperative agreement with the National Science Foundation

For M8 we extracted apertures of 6 pixels in the blue arm, and 5.45 pixels in the red one, in the spatial direction, which corresponds to an effective spatial resolution of 1″.2. This size was chosen as a compromise to have the maximum attainable spatial resolution (only slightly larger than the mean seeing of the night) and a good signal-to-noise ratio in the auroral lines of [O III] and [N II]. However, larger extractions of 4″.8 angular size were necessary to achieve a good flux measurement in the fainter O II RLs. Then, for the slit position 1 and considering the discarded apertures, we have obtained a final number of 150 apertures with a spatial resolution of 1″.2×0″.98 and 38 apertures with a resolution of 4″.8×0″.98 for the measurements of O II RLs. Similarly, a total number of 146 and 37 apertures were extracted, respectively, for the slit position 2. The smaller number of apertures obtained in this slit position is due to the fact that we discarded 4 apertures which were severely contaminated by stellar emission from Her 36.

In the case of NGC 7635 slit position, we extracted apertures with an angular size of 3″. A total of 30 apertures with an area of 3″×0″.98 were used. We also extracted individual integrated spectra of knots K1 and K2, and the rim of the bubble with areas of 12″.4×0″.98, 8″.5×0″.98 and 10″.4×0″.98, respectively. We notice the detection of the C II 4267 Å RL in the three extractions.

For M17, apertures extracted with an angular size of 1″.2 was sufficient to obtain a high signal-to-noise ratio in the auroral lines and RLs. We have obtained a total number of 185 apertures extracted with an individual area of 1″.2×0″.98.

Additionally, for each slit position, we extracted a one-dimensional spectra collapsing the whole slit –the sum of all the individual apertures. These are designated as "whole slit" spectra. The area covered by the "whole slit", and therefore the total extraction area, is shown in Fig. 1.

3 EMISSION LINE MEASUREMENTS AND REDDENING CORRECTION

The emission lines considered in our analysis were selected according to the following criteria:

- H I lines – Hα, Hβ and Hγ–, which are used to compute the reddening correction and to re-scale the line flux ratios of the red spectral range with respect to the blue one.
- CELs of several species in order to compute the physical conditions such as the auroral lines [O III] 4363 Å and [N II] 5755 Å used to derive the electron temperatures, [S II] 6717, 6731 Å and [Cl III] 5718, 5738 Å used to calculate the electron density.
- Other CELs needed to derive different ionic abundances (N^+, O^+, O^{2+}, S^+, S^{2+}, Cl^{2+} and Ar^{2+})
- Faint RLs of C II and O II, which are used to derive the C^{2+} and O^{2+} abundances and to compute the abundance discrepancy factor, ADF, for O^{2+} (via a comparison with the O^{2+} abundances derived from CELs).

Line fluxes were measured applying a single or a multiple Gaussian profile fit procedure over a local continuum. All these measurements were made with the SPLOT routine of the IRAF package and using our own scripts to automatize the process. Due to the local variations of the continuum

Table 1. Journal of observations.

Target	RA[a]	DEC[a]	PA (°)	Exposure time (s) Blue arm	Red arm
M8 POS1	$18^h03^m41\overset{s}{.}40$	$-24°22'42\overset{''}{.}7$	3	7×1200,60	36×180,60
M8 POS2	$18^h03^m40\overset{s}{.}42$	$-24°22'42\overset{''}{.}7$	0	7×1200,60	36×180,60
M17	$18^h20^m42\overset{s}{.}98$	$-16°10'02\overset{''}{.}4$	120	5×1800,60	15×500,60
NGC 7635	$23^h20^m44\overset{s}{.}36$	$+61°11'56\overset{''}{.}0$	67.5	5×1200,60	8×600,60

[a] Coordinates of the slit center (J2000.0).

around O II RLs and their faintness, these lines were measured manually.

Following Mesa-Delgado et al. (2008), to accurately compute the line fluxes we need to define the adjacent continuum of each line using the SPLOT routine. For each selected line, we define two small spectral zones at each side of the line as close as possible and free of any spectral feature. Then, the routine fits the continuum between both zones and the line profile to obtain the flux. The observational errors associated with the flux measurements were estimated following the criteria of Mesa-Delgado et al. (2008). The final error of a line flux was computed as the quadratic sum of the error in its flux measurement and the error in the flux calibration. All line fluxes for a given aperture were normalized to an H I line of reference, Hβ and Hα for the blue and red range, respectively.

The observed fluxes with respect to their H I line of reference were dereddened using the usual relation,

$$\frac{I(\lambda)}{I(\lambda_{ref})} = \frac{F(\lambda)}{F(\lambda_{ref})} 10^{c(\mathrm{H}\beta)\left[f(\lambda)-f(\lambda_{ref})\right]}, \qquad (1)$$

where the reddening coefficient, $c(\mathrm{H}\beta)$, represents the amount of interstellar extinction, $f(\lambda)$ the adopted extinction curve normalized to $f(\mathrm{H}\beta) = 0$, and λ_{ref} the H I line of reference. The reddening coefficient was determined from the comparison of the observed flux ratio of Hγ and Hα with respect to Hβ and the case B theoretical ones computed by Storey & Hummer (1995) for the physical conditions of T_e = 10000 K and n_e = 1000 cm^{-3}. The final $c(\mathrm{H}\beta)$ was the weighted average of the values obtained from each line. In appendix A, we present the dereddened emission line ratios and their associatted errors of the main emission lines per slit position as well as the observed Hβ flux and the mean $c(\mathrm{H}\beta)$ coefficient (just in the online version).

In all regions we have assumed the extinction law derived by Cardelli et al. (1989), which is parametrized by the ratio of total to selective extinction, $R_V = A_V/E(B-V)$. In the case of M17, NGC 7635 and the position 2 of M8, we have used the typical value in the diffuse interstellar medium, $R_V = 3.1$. For the position 1 of M8 we have adopted different values of R_V depending on the zones covered by the slit. It is well known that the main ionization source of HG is Her 36 (Woodward et al. 1986) and that it shows a considerably higher extinction than the other zones of M8, which are mainly ionized by 9 Sgr and most of their reddening is due to foreground interstellar dust. Consequently, following Sánchez & Peimbert (1991) we have adopted a $R_V = 5.0$ to correct the apertures of position 1 that cover the HG region (the area indicated by a darker grey band in the slit position 1 of M8 shown in Fig. 1) and the typical value $R_V = 3.1$ in the other zones. The use of a higher total to selective extinction produces significant changes in the $c(\mathrm{H}\beta)$ values, while the line flux ratios remain almost unaffected by deviations from the classical extinction law. In the case of the "whole slit" spectra, we have also assumed the typical R_V value for the interstellar medium. Finally, in order to produce a final homogeneous set of dereddened flux ratios, all of them were re-scaled to Hβ. The re-scaling factor used in the red spectra was the theoretical Hα/Hβ ratio for the physical conditions of T_e= 10000 K and n_e= 1000 cm^{-3}. The final error associated with the line dereddened fluxes include the uncertainties in the flux measurements, flux calibration and the error propagation in the reddening coefficient.

In the different panels of Fig. 2 we present the spatial profiles of the $c(\mathrm{H}\beta)$ determinations as a function of the positional measurement along the slit in arcseconds. Hereinafter, each positional measurement represents the position on the slit of a given quantity obtained for an individual extraction with origin in the south edge of the original slit in the case of M8, in the northwest edge for M17 and in the southwest edge for NGC 7635. In all cases, we have found a good agreement between our determinations and those available in the literature, considering that the measurements do not correspond exactly to the same spatial zone and the areas covered by the slits are also different. On the one hand, Figs 2(a) and 2(b) show the spatial distribution of $c(\mathrm{H}\beta)$ for slit positions 1 and 2 of M8, respectively, where we can notice higher $c(\mathrm{H}\beta)$ values associated with the HG region and the zones near Her 36. These values are in agreement with previous $c(\mathrm{H}\beta)$ determinations carried out in the HG region by Sánchez & Peimbert (1991), Esteban et al. (1999) and García-Rojas et al. (2007), who found values between 0.85 and 1.0 dex. On the other hand, in Fig. 2(c) we present the spatial distribution of $c(\mathrm{H}\beta)$ along the slit position of M17. We have compared our determinations with those performed by Peimbert et al. (1992), whose slit positions 3 and 13 approximately coincide with the positional measurements 60″ and 125″, respectively. For those positions, Peimbert et al. (1992) obtained values of about 1.72 and 1.45 dex, which are in agreement with our determinations considering the uncertainties in the $c(\mathrm{H}\beta)$ determination. Fig. 2(d) presents the $c(\mathrm{H}\beta)$ spatial profile of NGC 7635. In this panel, we can see higher $c(\mathrm{H}\beta)$ values related to the knots and the rim. We have compared our values with previous determinations obtained by Talent & Dufour (1979) and Moore et al. (2002) at different parts of the nebula. Positions 3 and 5 of Talent & Dufour (1979) coincide with the positions of the knot K1 and the rim indicated in Fig. 2(d). Talent & Dufour (1979) measured $c(\mathrm{H}\beta)$ values at those positions of about 1.21 and 1.07 dex, respectively, which are in agreement with our determinations. On the other hand, Moore et al. (2002)

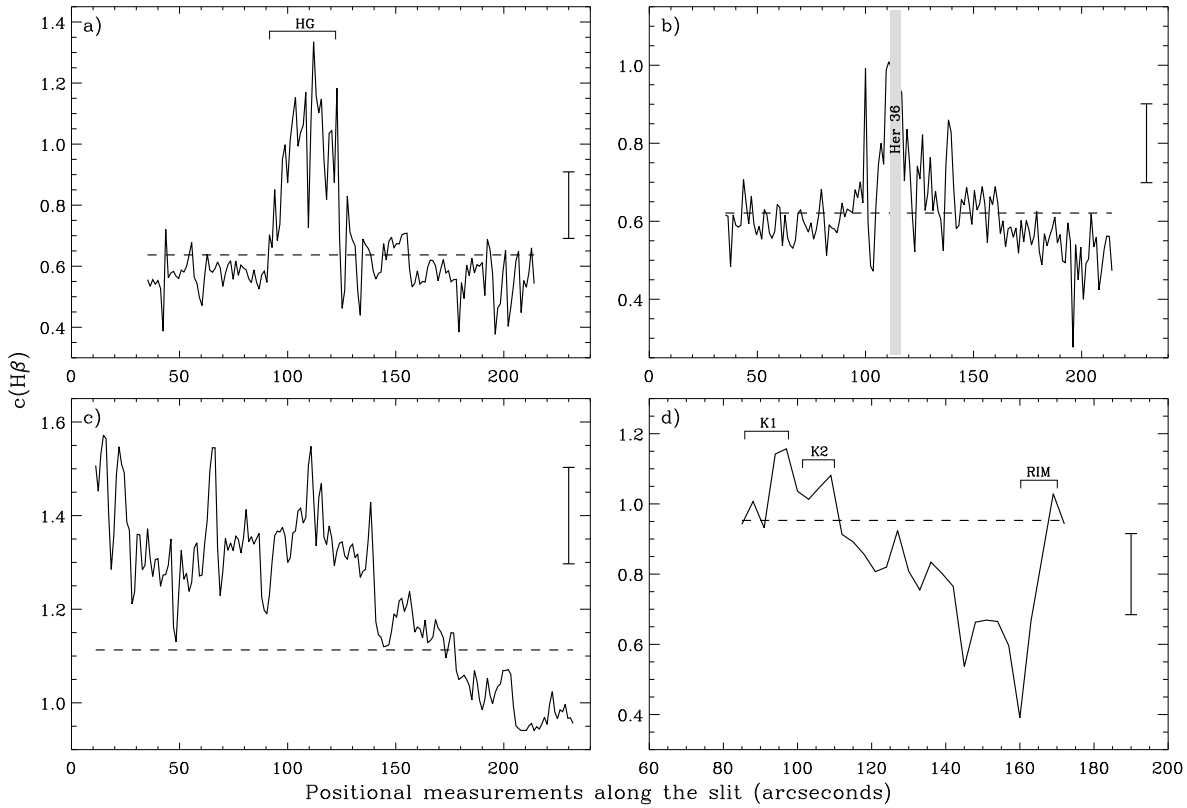

Figure 2. Spatial profiles of the reddening coefficient, $c(\mathrm{H}\beta)$, along the slit positions: a) M8 POS1, b) M8 POS2, c) M17 and d) NGC 7635. The position of the Hourglass region (HG) as well as of the knots K1, K2 and the rim of the bubble of NGC 7635 are indicated. The grey band in b) corresponds to apertures contaminated by stellar emission from Her 36. Positional measurements along the slits go from south to north in the two positions of M8 and from the west to east for M17 and NGC 7635. The dashed horizontal line represents the $c(\mathrm{H}\beta)$ value obtained for the "whole slit" spectra. The typical error bar is also included.

obtained a similar value, 1.25 dex, from their slit position that covers the knots K1 and those located to the south of K1, but measured a value of about 1.46 dex for the rim of the bubble, which is higher than our determination and that of Talent & Dufour (1979) at the same position. The typical error in the $c(\mathrm{H}\beta)$ coefficient presented in Fig. 2 is of about 0.1 dex for all regions.

The results shown in Fig. 2 indicate that an important fraction of the extinction should come from dust located inside the objects, and that the distribution of such absorbing material is not homogeneous.

4 PHYSICAL CONDITIONS AND CHEMICAL ABUNDANCES

4.1 Physical conditions

We have determined the physical conditions –electron densities and temperatures– from the usual CEL ratios and using the IRAF task TEMDEN of the NEBULAR package (Shaw & Dufour 1995) with updated atomic data (see Liu et al. 2000; García-Rojas et al. 2005). We have computed the electron density, n_e, from the [S II] 6717/6731 line ratio and the electron temperatures, T_e, from the nebular to auroral [O III] (4959+5007)/4363 and [N II] (6548+6584)/5755 line ratios. Although we detect the [Cl III] doublet in several apertures, we do not use these lines to obtain density values due to their large associated errors. The spatial distributions of the physical conditions are presented and discussed for each region in §5.

Following the same methodology as Mesa-Delgado et al. (2008) for the determination of the physical conditions, a representative initial T_e = 10000 K is assumed in order to derive a first approximation of n_e([S II]) –hereinafter n_e. Then, we calculate T_e([O III]) and T_e([N II]), and iterate until convergence to compute the finally adopted values using T_e([N II]) in the density calculations. The errors in the physical conditions were computed by error propagation on the analytical expressions of n_e by Castañeda et al. (1992) and those of T_e given by Osterbrock & Ferland (2006) (their equations 5.4 and 5.5). Although the expression derived by Castañeda et al. (1992) is only valid to a limited range of densities lower than 10^4 cm^{-3}, and uses the old atomic data for S^+ from the compilation by Mendoza (1983), it seems adequate for an estimation of the errors in the physical conditions.

4.2 Ionic abundances from CELs and RLs

We used the IRAF package NEBULAR in order to derive ionic abundances of N^+, O^+, O^{2+}, S^+, S^{2+}, Cl^{2+} and Ar^{2+} from CELs. We have assumed no temperature fluctuations in the

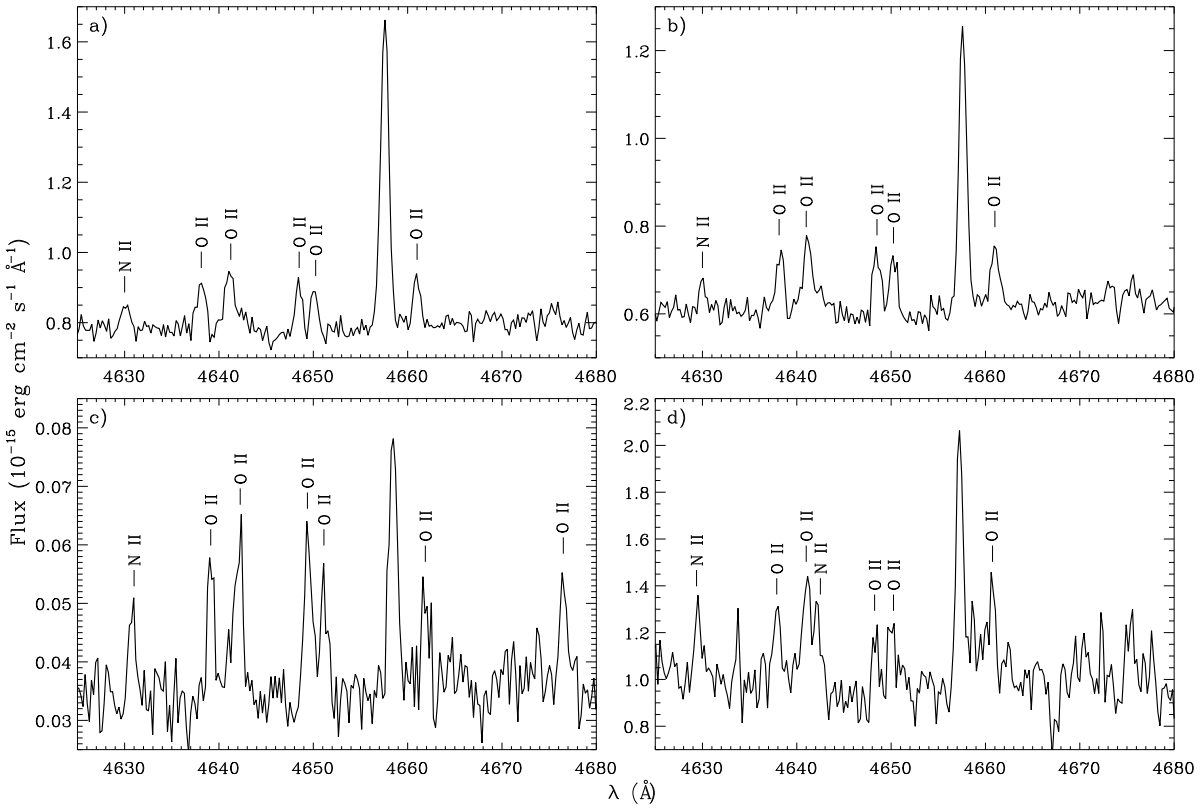

Figure 3. Sections of the spectrum around the emission lines of multiplet 1 of O II. Panels a) and b) correspond to apertures of 4.″8 wide extracted from slit positions 1 and 2 of M8, respectively, extending from positional measurements 137.″2 to 142″. Panel c) corresponds to an 1.″2 wide aperture extracted from the slit position of M17, which covers from 153.″4 to 154.″6. Panel d) shows a section of the "whole slit" spectrum of NGC 7635.

ionized gas (t^2= 0) and a two-zone scheme, adopting the T_e([N II]) to derive the abundances of singly ionized species and T_e([O III]) in the case of doubly ionized species. The electron density obtained from the[S II] line ratio was adopted for all ionic species. The errors in the ionic abundance determinations were calculated as the quadratic sum of the independent contributions of temperature, density, and line flux uncertainties. The spatial distributions of the ionic abundances of some species are presented and discussed for each region in §5.

The wavelength range covered with the blue arm did not include the bright [O II] 3726, 3729 Å lines. In the case of NGC 7635, it was necessary to determine the O^+ abundance (see §6); to do that, we performed a proper subtraction of the telluric emission in the [O II] 7320, 7330 Å lines. The subtraction was achieved using re-scaled pure telluric measurements from sky extractions of different sizes of long exposure spectra of a compact H II region observed during the same night (the data of this object were published in Martín-Hernández et al. 2008). This procedure adds an uncertainty between 6% and 8% higher in the flux measurements of [O II] lines. On the other hand, in the cases of M8 and M17 we consider not necessary to determine the O^+ abundance for our aims.

We have detected and measured pure RLs of the multiplet 1 of O II (see Fig. 3) and C II 4267 Å. The abundance of a heavy element X in the ionization state $i+1$, that emits a RL at wavelength λ is given by

$$\frac{N(X^{i+1})}{N(H^+)} = \frac{\lambda(Å)}{4861}\frac{\alpha_{eff}(H\beta)}{\alpha_{eff}(\lambda)}\frac{I(\lambda)}{I(H\beta)}, \qquad (2)$$

where $I(\lambda)/I(H\beta)$ is the dereddened flux ratio, $\alpha_{eff}(\lambda)$ and $\alpha_{eff}(H\beta)$ are the effective recombination coefficients for the RL and Hβ, respectively. Due to the similar temperature dependence of the emissivities of RLs, the $\alpha_{eff}(H\beta)/\alpha_{eff}(\lambda)$ ratio is almost independent of the adopted temperatures. In our case, under the two-zone scheme, we have assumed T_e([O III]) to calculate the C^{2+} and O^{2+} abundances.

We have detected the C II line at 4267 Å in most of the apertures extracted at 1.″2 in M17 and M8, and in the integrated spectra for the "whole slit", the knots and the rim of the bubble of NGC 7635 (see §6). C^{2+} abundances from RLs have been calculated using the atomic data of Davey et al. (2000).

The O^{2+} abundances were derived when at least four lines of multiplet 1 were measured in a given one-dimensional spectrum using the effective recombination coefficients from Storey (1994) and the same method that is detailed in Esteban et al. (1998). We have determined the O^{2+} abundances correcting for the departure from local thermodinamyc equilibrium (LTE) of the upper levels of the transitions of multiplet 1 of O II for densities lower than 10000 cm^{-3} using the empirical formulation proposed by Peimbert & Peimbert (2005). Abundances determined assuming LTE for the population of the levels do not differ more than a 2% from

the NLTE ones because we use several of the brightest lines of the multiplet. We have computed the O^{2+}/H^+ ratio for 89% of the apertures extracted at 1.″2 in M17, for all the apertures extracted at 4.″8 in both slit positions of M8, and in the "whole slit" spectrum of NGC 7635 (see §6).

5 SPATIAL PROFILES ALONG THE SLIT POSITIONS

In the following sections we present the spatial profiles of several nebular properties along the slit positions of each H II region. The selected parameters were: n_e, T_e([N II]), T_e([O III]), the flux of several selected lines ([Fe III] 4658 Å, C II 4267 Å, O II 4649 Å and [O III] 4959 Å), and the O^{2+} abundances obtained from CELs and RLs.

5.1 M8

In Figs 4 and 5 we show the spatial variations of the nebular properties for the slit positions 1 and 2 of M8, respectively.

The spatial profiles of n_e along the slits show a wide range of variation with a maximum associated with the HG region in position 1 (see Fig. 4a) and the apertures near Her 36 in the case of position 2 (see Fig. 5a). The density peak in Fig. 4(a) associated with HH 870 reaches a value higher than 800 cm^{-3}. Following the nomenclature proposed by Arias et al. (2006), that peak would be more specifically related to the knot B of this object. At the HG region we find densities between 2600 and 3500 cm^{-3}, values which are in agreement with previous determinations by García-Rojas et al. (2007) and Peimbert et al. (1993), who derive densities between 1800 and 3700 cm^{-3}. We have noticed a slight localized enhancement of about 300 cm^{-3} in the density profile of position 1 around the positional measurement 155.″2 (indicated as HH? in Figs 1 and 4). This feature coincides in Fig. 1 with a relatively bright rim crossed by the slit and located about 45″ to the north of the centre of the HG region. In §7.3 we argue that this feature may be a candidate to HH object. In Fig. 5(a), the highest density value is related to an ionization front located at 15.″3 S and 1.″5 E from Her 36. In this slit position, we have also detected local maxima at the positional measurements 65.″2, 79.″6, 151.″6 and 192.″4. On the one hand, the first two maxima coincide in Fig. 1 with gaseous arcs that surround faint stars located approximately at 34″ and 49″ to the south of Her 36. On the other hand, the other maxima are related to high density filaments located approximately at 40″ and 80″ to the north of Her 36. The average value of both slit position 1 and 2 obtained from the "whole slit" spectrum, and included in panel (a) of Figs 4-5 with dashed line, amounts to 1140±220 and 750±150 cm^{-3}, respectively.

The spatial profiles of T_e([O III]) and T_e([N II]) are presented in the panels (b) of Figs 4 and 5 for the slit positions 1 and 2, respectively. We do not find relevant features in these profiles, excluding perhaps very slight enhancement of both temperature indicators at the HG region. However, the temperature rise at these positional measurements are of the order of the error bar. We also present the T_e([N II])/T_e([O III]) ratio in the bottom panels of Figs 4(b) and 5(b), which is basically constant along the slits showing spatial variations of the order of the observational errors. In general, T_e([N II]) is slightly higher than T_e([O III]), a typical result obtained for H II regions as a consequence of the hardening of the radiation field in the low ionization zones (e.g. Stasińska 1980).

One of the main spectral properties of HH objects is their strong emission in [Fe III] lines due to the destruction of dust grains (Mesa-Delgado et al. 2009) or changes in the ionization conditions (Blagrave et al. 2006). In Figs 4(c) and 5(c) we have plotted the spatial profile of the dereddened flux of [Fe III] 4658 Å with respect to Hβ for the slit positions 1 and 2, respectively. In the slit position 1 we can see a clear rise of the flux at the position of HH 870, which increases by a factor of ∼2 with respect to the adjacent background gas. This factor seems to extend along the HG region where the ionization degree decreases and the electron density increases. As in the density spatial profile of slit position 1, we have found in Fig. 4(c) an enhancement of the [Fe III] emission line at the positional measurement 155.″2 where a possible candidate to HH object is located (see §7.3). In the case of the slit position 2, we have found no evidence of important localized increase in the [Fe III] emission, only a decrease of a factor of 2 around Her 36.

In Figs 4(d)–5(d) and 4(e)–5(e) the spatial profiles of the observed flux of C II 4267 Å, O II 4649 Å, and [O III] 4959 Å lines along the slit positions are shown, as well as their ratio in the bottom panels of the same figures. It should be reminded that the extractions of the O II line are 4.″8 wide. Then, each extracted aperture represents the average value of four apertures extracted with a spatial size of 1.″2. In order to perform a proper comparison, we have also plotted the observed fluxes of C II and [O III] lines with extractions 4.″8 wide. The spatial distributions of the pure RLs are quite similar in each slit position. However, we can note a slight rise of the F(C II 4267 Å)/F(O II 4649 Å) ratio at the HG and HH 870 regions (see Fig. 4d). We have observed a similar enhancement of the ratio of emission lines of species with similar ionization potential to C^{2+} (24.4 eV), like Ar^{2+} (27.6 eV) or Cl^{2+} (23.8 eV), with respect to [O III] 4959 Å and O II 4649 Å. In order to explore the reason of this enhancement, we have determined the spatial distribution of the ionization degree which presents an inverse behaviour to the C II/O II ratio. Though we have not subtracted the telluric emissions from [O II] 7320, 7330 Å lines in M8, we have observed that the O^{2+}/O^+ decreases between the positional meassurements at 70″ and 130″, where the HG region is located, reaching values of about −0.4 dex lower than in the rest of the slit position. Therefore, this indicates that the variation in the C II/O II ratio can be simply due to the decrease of the ionization degree in that zone. On the other hand, the point-to-point comparison of the spatial profiles of [O III] 4959 Å and O II 4649 Å (see Figs 4e–5e) does not show clear tendencies.

The [O III] spatial distribution of the slit position 1 and 2 of M8 suggests that the gas covered by both slits might not be ionized by the same source. Slit position 1 shows a [O III] emission distribution rather similar to the density distribution, but position 2 does not. In fact, the [O III] emission shows a peak at the ionization front at the south of Her 36 (positional measurement ∼95″) and remains almost constant toward the north of the slit. This area coincides with the dark zone around Her 36. It seems that while the HG region and the area at the south of the positional mea-

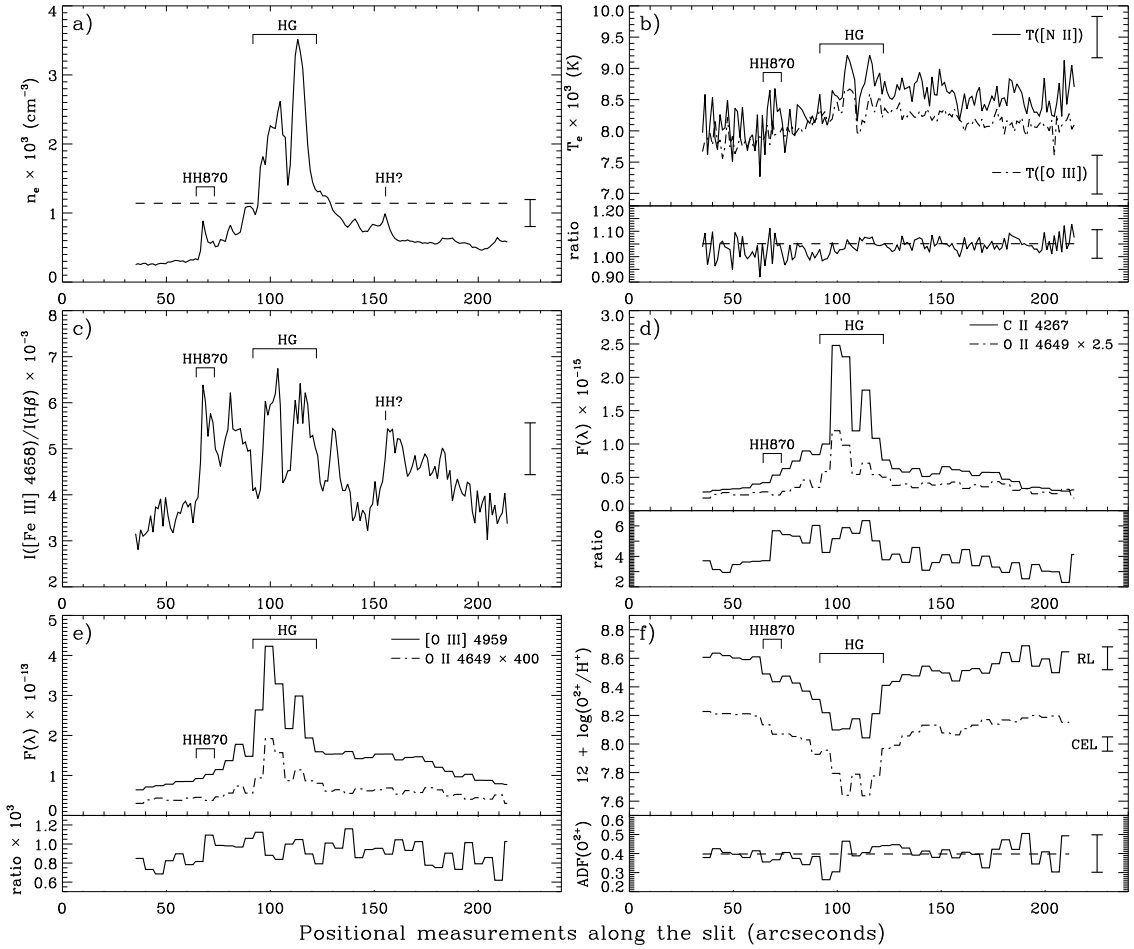

Figure 4. Spatial profiles of several nebular parameters along the slit position 1 of M8. Positional measurements along the slit go from south to north (see Fig. 1). The position of the Hourglass (HG) region and the HH object 870 are indicated as well as the typical error of some variables. The possible candidate to HH object (see §7.3) is also marked as HH? in panels (a) and (c). The horizontal dashed line in some panels indicates the value obtained for the "whole slit" spectrum. (a) Profile of n_e; (b) top: profiles of T_e([N II]) (solid line) and T_e([O III]) (dash-dotted line), botton: profile of the T_e([N II])/T_e([O III]) ratio; (c) profile of the dereddened flux ratio of [Fe III] 4658 Å; (d) top: observed flux of C II 4267 Å (solid line) and O II 4649 Å (dash-dotted line), botton: profile of the F(C II 4267 Å)/F(O II 4649 Å) ratio; (e) top: observed flux of [O III] 4959 Å (solid line) and O II 4649 Å (dash-dotted line), botton: profile of the F([O III] 4959 Å)/F(O II 4649 Å) ratio; (f) top: O^{2+} abundances from RLs (solid line) and CELs (dash-dotted line), botton: profile of ADF(O^{2+}). All observed fluxes have units of erg cm^{-2} s^{-1}. Note that from panel a) to c) the profiles correspond to extractions of 1.″2. From panels d) to f) the spatial increments are 4.″8 wide.

surement ∼95″of the slit position 2 are ionized by Her 36, the rest of the position 2 is ionized by another star, perhaps 9 Sgr. This hypothesis is consistent with the results from previous works of Woodward et al. (1986) and Sánchez & Peimbert (1991).

Finally, Figs 4(f)–5(f) show the spatial variation of the O^{2+} abundances derived from RLs and CELs, as well as the AD factor of this ion –ADF(O^{2+})– defined in its logarithmic form as

$$\mathrm{ADF(O^{2+}) = } log(\mathrm{O^{2+}/H^+})_{\mathrm{RLs}} - log(\mathrm{O^{2+}/H^+})_{\mathrm{CELs}}. \quad (3)$$

As in Figs 4(d)–(e) and 5(d)–(e), we present the spatial profile for the extractions 4.″8 wide of the O^{2+}/H^+ ratio obtained from RLs and CELs. The ADF(O^{2+}) remains fairly constant along the slit positions 1 and 2 with average values of 0.40±0.11 and 0.37±0.09 dex, respectively, which are in agreement with previous determinations obtained by Esteban et al. (1999) –0.34 dex– and García-Rojas et al. (2007) –0.37 dex. The only relevant variation detected in the O^{2+} abundance profiles is at the HG region, where the O^{2+} abundance decreases up to 7.6 dex due to the decrease of the ionization degree.

5.2 M17

Fig. 6 shows the spatial distributions of several nebular properties along the slit position that covers two bright areas of M17 (see Fig. 1). The density profile (Fig. 6a) shows a peak between the positional measurements 30″ and 90″, a rather constant value between 90″ and 180″ and a decrease at the eastern edge. We have found a good agreement between our density determinations and those at the positions 3 and 13 studied by Peimbert et al. (1992), which coincide with our positional measurements 60″ and 125″ (see §3). In the case of the temperature distributions (see Fig. 6b), we only have

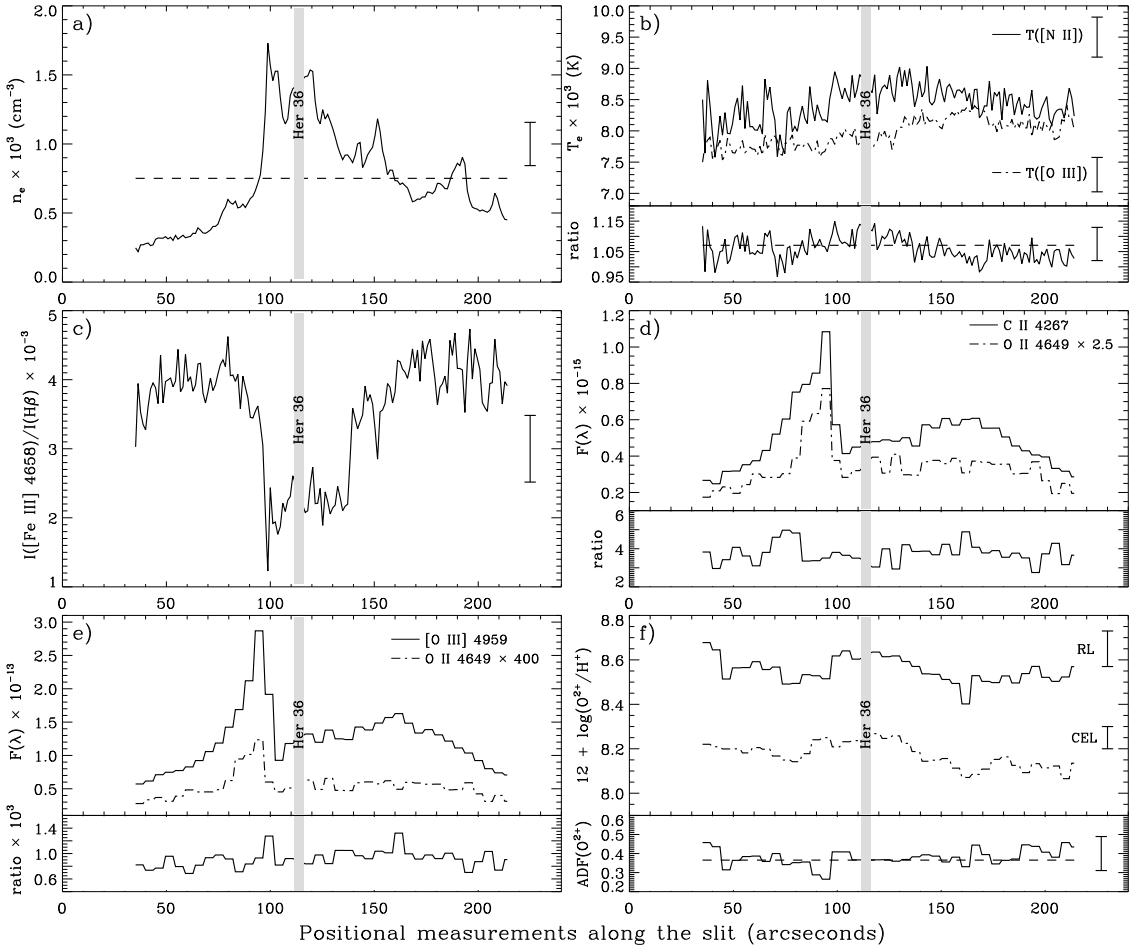

Figure 5. Same as Fig. 4 for the slit position 2 of M8. The grey vertical band covers the apertures affected by stellar features from the emission of Her 36.

found variations of the order of our error bar. In the case of the T_e([O III]), we have found values similar to those derived by Peimbert et al. (1992) in their slit positions. On the other hand, the T_e([N II]) obtained by those authors shows a higher value at their position 3, which amounts to 11600 K. However, Esteban et al. (1999) also explored the physical conditions at position 3 of Peimbert et al. (1992) and found a T_e([N II]) of about 8990 K, which is in agreement with our determinations within the errors. In Fig. 6(c), we can find the spatial profile of the [Fe III] 4658 Å line flux with respect to Hβ, where we do not find any localized enhancement, which may be related to the presence of HH objects.

The spatial distributions of the C II 4267 Å and O II 4649 Å are presented in Fig. 6(d), where we can notice an increase of the C II emission flux to the east of the positional measurement 140″. This rise can be related to a decrease of the ionization degree. In fact, Peimbert et al. (1992) find a change in the O^{2+}/O^{+} ratio between their slit positions 3 and 13 of about 0.40 dex. The comparison of the [O III] and O II emission line fluxes in Fig. 6(e) does not show relevant features, and their ratio remains essentially constant along the slit.

Finally, Fig. 6(f) shows the spatial profiles of the O^{2+} abundances derived from RLs and CELs, as well as their ratio, ADF(O^{2+}). As we can see, both abundance determinations show a similar decrease along the slit, while the ADF(O^{2+}) distribution present a constant value of about 0.37±0.09 dex. This value is somewhat higher than that obtained in the "whole slit" spectrum, which amounts to 0.31±0.07 dex, although the difference is consistent within the errors.

5.3 NGC 7635

The spatial distributions of nebular properties along the slit position of NGC 7635 are presented in Fig. 7. Each positional measurement corresponds to an area of 3″×0.″98. The results obtained for the integrated spectra covering separately the bright knots at the west of the central star, K1 and K2, and the rim of the bubble (see Fig. 1) are presented in §6.

In Fig. 7(a) the density profile shows its highest value at the position of knot K1, where it reaches a value of about 2600 cm^{-3}. Rodríguez (1999) obtained the density in three zones of NGC 7635 and her position 1 coincides with our K1, as well as the slit position 3 of Talent & Dufour (1979). Rodríguez (1999) derived a density value of about 2800 cm^{-3}, which is in agreement with our results, while Talent & Dufour (1979) derived a density value of about 4200 cm^{-3}. Moreover, Moore et al. (2002) also obtained a

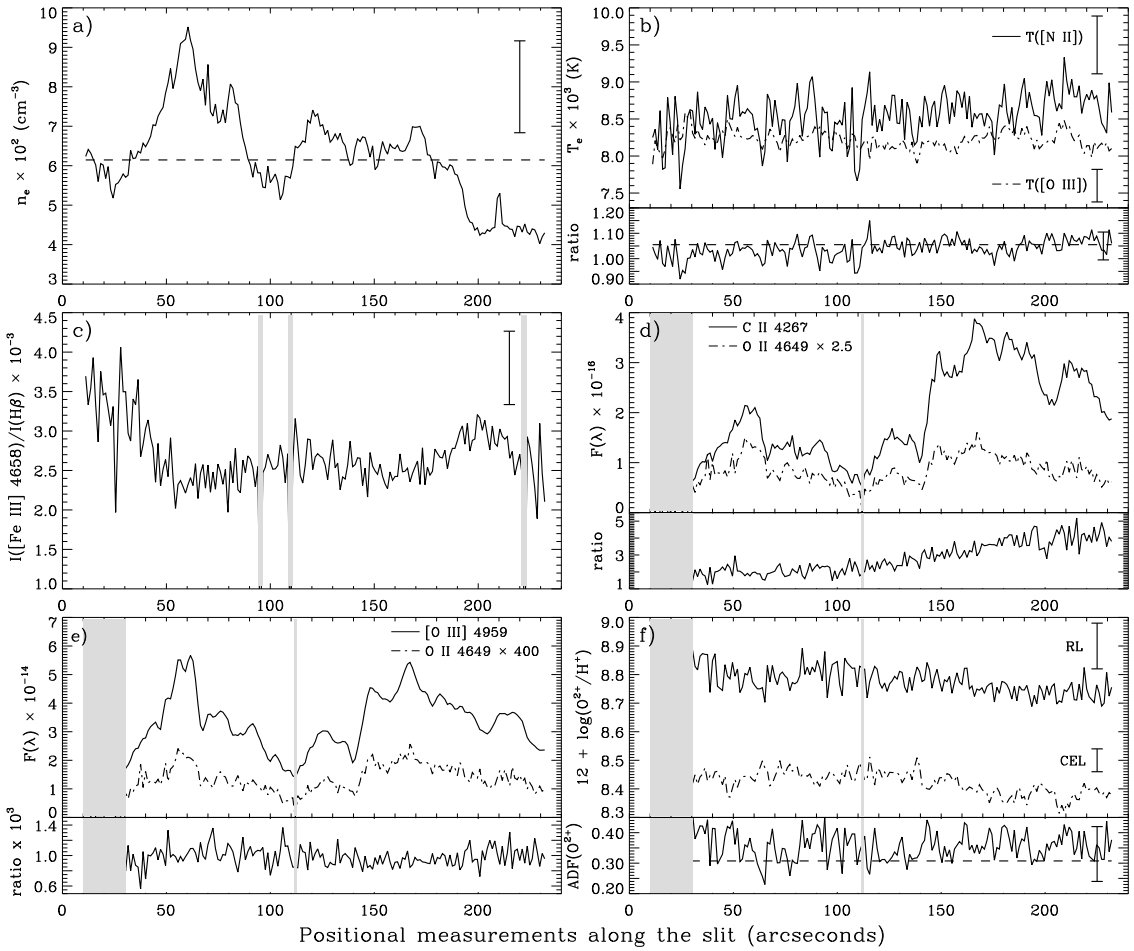

Figure 6. Same as Fig. 4 for the slit position of M17. The grey bands cover apertures where [Fe III] 4658 Å (c) and O II 4649 Å (d–f) were not detected. Positional measurements along the slit go from west to east (see Fig 1).

higher density values on the knots and the rim, but with larger uncertainties. Two local maxima can also be seen at the positional measurements corresponding to the knot K2 and the rim. Between the knots and the rim, the density remains rather constant with an average value of about 100 cm^{-3} and a standard deviation of about 20 cm^{-3}.

In Fig. 7(b), we can see that the electron temperatures do not show strong variations along the slit and are of the order of the error bar. The average values of both temperatures amount to 8600 K for T_e([O III]) and 8100 K in the case of T_e([N II]) with standard deviations of about 390 K and 420 K, respectively. Their ratio shows an average value of 0.94 with a standard deviation of about 0.05. Our temperature determinations are in agreement with the results of Rodríguez (1999), Talent & Dufour (1979) and Moore et al. (2002).

Fig. 7(c) shows the spatial profiles of the dereddened fluxes of [O III] 5007 Å and [O II] 7320 Å with respect to Hβ and normalized to their respective maximum emission. On the one hand, the [O II] spatial profile shows its maximun values at the position of the knot K1 decreasing progressively up to the positional measurement 110″. On the other hand, the [O III] distribution presents an inverse pattern with a progressive increase until the same positional measurement. Beyond this point, both spatial profiles do not show strong variations. A similar result can be seen in the *HST* images of Moore et al. (2002). The behaviour shown in Fig. 7(c) is due to a dramatic change of the ionization degree. The knots have a lower ionization degree than the gas beyond the positional measurement 110″, which corresponds to the bubble.

Finally, Fig. 7(d) shows the heliocentric radial velocity, V$_{hel}$, spatial distribution obtained from the Gaussian fit of the Hα line profile. We have obtained the most negative velocity at the position of the rim, which is about −54±4 and in agreement with the mean heliocentric velocity found by Christopoulou et al. (1995) for NGC 7635. This value is also similar to that of the molecular cloud associated to the bubble and the S162 complex (see Christopoulou et al. 1995, and references therein). The expansion of the bubble is very slow, with velocities between 4 and 25 km s^{-1}and, therefore, our spectral resolution did not allow us to resolve the line splitting of the expanding bubble. In fact, the velocity profile along the slit shown in Fig. 7(d) does not show any remarkable feature or velocity differences substantially larger than the uncertainties.

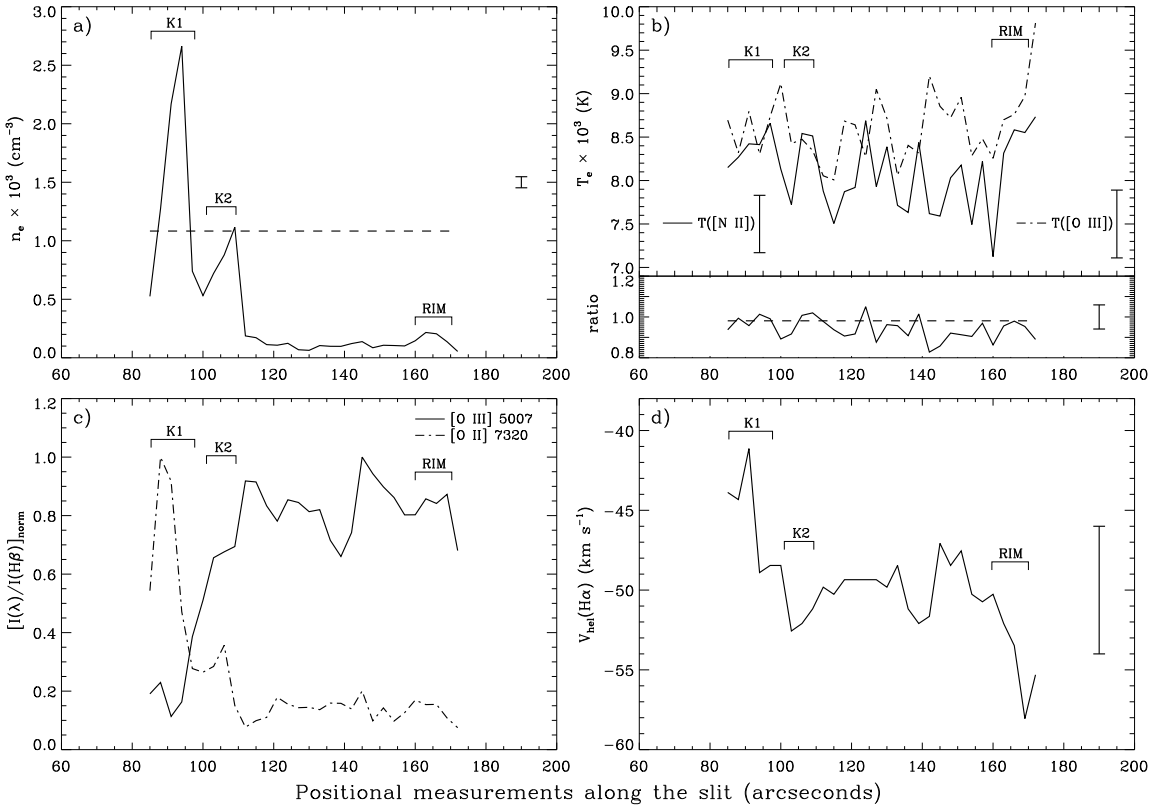

Figure 7. Spatial profiles of several nebular properties along the slit position of NGC 7635. Positional measurements along the slit go from west to east (see Fig 1). The position of the knots, K1 and K2, and the RIM are indicated as well as the typical error of some variables. The horizontal dashed line in some panels gives the value obtained from the "whole slit" spectrum. (a) Profile of n_e; (b) top: profiles of T_e([N II]) (solid line) and T_e([O III]) (dash-dotted line), botton: profile of T_e([N II])/T_e([O III]) ratio; (c) profile of the dereddened fluxes with respect to Hβ of [O III] 5007 Å (solid line) and [O II] 7320 Å (dash-dotted line) normalized to their respective maximum; (d) heliocentric velocity profile obtained from the centroid of Hα.

Table 2. Physical conditions and ionic abundances[a] of selected zones of NGC 7635.

				"Whole Slit"	
	K1	K2	RIM	$t^2 = 0$	$t^2 > 0$
n_e([S II]) (cm^{-3})	1900±150	890±70	180±30	1080±90	
T_e([N II]) (K)	8450±320	8150±300	8680±430	8420±330	
T_e([O III]) (K)	8830±800	8140±290	8640±320	8580±320	
C^{2+b}	8.21±0.14	8.46±0.08	8.40±0.12	8.44±0.12	
N^+	7.55±0.04	7.27±0.04	6.87±0.05	7.32±0.04	7.66±0.06
O^+	8.39±0.10	8.28±0.10	7.97±0.12	8.24±0.10	8.45±0.17
O^{2+}	7.32±0.10	8.07±0.05	8.08±0.05	7.89±0.05	8.48±0.08
O^{2+b}	–	–	–	8.48±0.09	
S^+	6.37±0.04	6.06±0.04	5.53±0.04	6.10±0.04	6.43±0.06
S^{2+}	6.69±0.20	6.90±0.09	6.71±0.09	6.77±0.09	7.40±0.12
N^+/O^+	−0.84±0.11	−1.02±0.11	−1.10±0.13	−0.91±0.11	−0.79±0.18
O^{2+}/O^+	−1.07±0.15	−0.21±0.11	0.11±0.13	−0.34±0.11	0.03±0.19
S^+/O^+	−2.02±0.11	−2.23±0.11	−2.44±0.13	−2.14±0.11	−2.02±0.18

[a] In units of $12+log(X^{+i}/H^+)$.

[b] Determined from RLs.

6 CHEMICAL ABUNDANCES OF SELECTED ZONES OF NGC 7635

In this section, we present the physical conditions and ionic and elemental abundances –derived from CELs and RLs– obtained from the integrated spectra that cover the knots –K1 and K2, the rim of the bubble as well as the "whole slit" spectrum. The results are shown in Tables 2 and 4.

The physical conditions derived from the ratios of CELs are shown in Table 2. These values are in agreement with those obtained from the 3″ extractions presented in Fig. 7, as well as with the different determinations of the literature that we have cited in §5.3. We can notice that the temperatures calculated from the different indicators are very similar within the errors, in agreement with the result obtained from the temperature spatial distribution along the slit position (see Fig. 7b). The electron density and temperatures found for the "whole slit" spectra are basically averages of the knots and the rim values.

We have derived ionic abundances of several ions (see Table 2). The O^+/H^+ ratio was obtained removing the telluric contamination from the [O II] 7320, 7330 Å lines as it was explained in §4.2. A proper determination of the O^+ abundances has allowed us to explore the strong variation of the ionization degree between the knots and the rim. As we can see in Table 2, the ions with low ionization potential, such as N^+, O^+ and S^+, show a gradual decrease in their abundance following the sequence: K1, K2 and the rim. As it is expected, this decrease is accompanied by an increase of the abundances of ions of high ionization potential, however the differences between K2 and the rim are not large in this case. In Fig. 8 we present the spatial distribution of several emission lines of ions with different ionization potentials: S^+ (10.4 eV), H^+ (13.6 eV) and O^{2+} (35.1 eV). The profiles are centered around the knots (Fig. 8a) and the rim (Fig. 8b). As it is shown in Fig. 8(a), the [O III] profile shows a completely different behaviour with respect to the other ions showing a progressive decrease from the positional measurement 110″ towards the west (left in Fig. 8a). This behaviour is produced because most ionizing photons which are able to convert O^+ to O^{2+}, are exhausted between the positional measurement 105″ and 110″ and, therefore, they do not get to penetrate the inner surface of K1, which is facing the ionizing star. Then, K1 is a wall of dense material that maintains the nebula ionization-bounded at that precise location. In the case of K2, the spatial profiles of the three emission lines are rather similar, indicating that this feature is matter-bounded or conversely, it is a ionization front which surface is perpendicular to the line of sight. Finally, the behaviour of the line profiles at the rim –whose surface is tangential to the line of sight– indicates that it is a matter-bounded feature. This is also consistent with the fact that T_e([O III]) and T_e([N II]) are so similar at the rim.

It is important to note that we have detected and measured the faint C II 4267 Å RL (see Fig. 9) in all the integrated spectra, as well as five of the eight RLs of the multiplet 1 of O II (see Fig. 3d) in the "whole slit" spectrum, allowing us to derive C^{2+} and O^{2+} abundances from RLs. Several authors have previously determined the C^{2+} abundance in NGC 7635. Rodríguez (1999) obtained values between 8.11 and 8.23 dex in her two slit positions which cover the group of knots at the south of K1. On the bubble rim, Moore et al. (2002) obtained a C^{2+} abundance of 8.63 dex. Our determinations lie in between those values. In addition, Moore et al. (2002) obtained the first determination of the O^{2+}/H^+ ratio from RLs on the rim bubble, they found a value of 8.47 dex and a moderate ADF(O^{2+}) = 0.2 dex. However, from our "whole slit" spectrum we obtain an ADF(O^{2+}) of about 0.59±0.10 dex, the highest value found so far in an H II region (see §7.1).

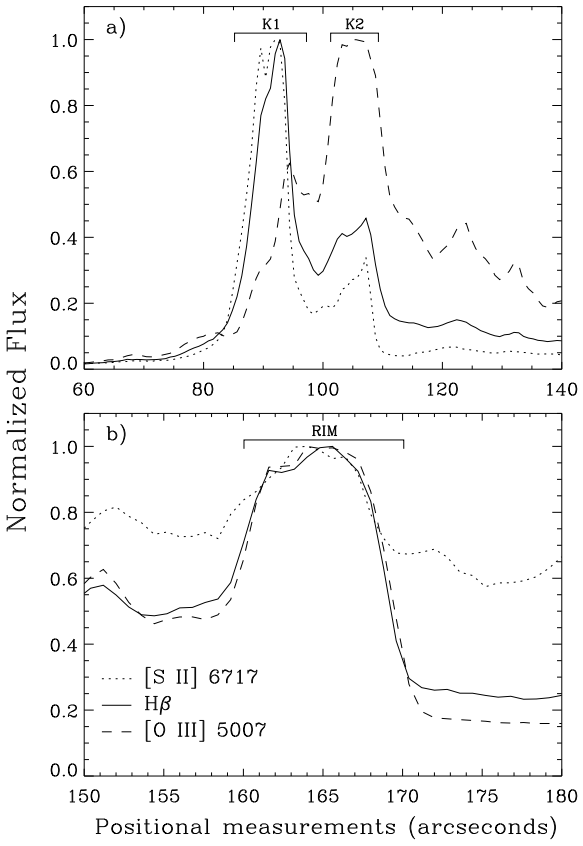

Figure 8. Spatial profiles of several emission lines obtained from extractions with a size of 0.″8 –the average seeing during the observations– around the knots (a) and the rim (b).

In order to derive the total gaseous abundances of the different elements, we have corrected for the unseen ionization stages by using a set of ionization correction factors (ICFs). Both adopted ICF values and total abundances are presented in Table 3 and Table 4, respectively. For carbon, we have adopted the photoionization models of Garnett et al. (1999) to estimate the ICF(C^+). In the case of oxygen and nitrogen, we considered the classical assumptions $O = O^+ + O^{2+}$ and $N^+/N = O^+/O$, respectively. Finally, we have used the relation proposed by Stasińska (1978) to derive the ICF(S^{3+}) and the S abundances. In general, the total abundances derived for K1 and K2 are rather similar considering the uncertainties –except perhaps in the case of carbon– but higher than those derived for the spectrum of the rim. For the knots, Rodríguez (1999), Talent & Dufour (1979) and Moore et al. (2002) determine a total O abundance of about 8.42, 8.72 and 8.78, respectively. Our O abundance determinations for K1 and K2 are only consistent

Table 3. Set of ionization correction factors adopted in NGC 7635.

Elements	Unseen ion	K1	K2	RIM	"Whole Slit" $t^2=0$	"Whole Slit" $t^2>0$
C	C^+	6.20±1.94	2.03±0.55	1.56±0.50	2.34±0.66	1.64±0.74
N	N^{2+}	1.09±0.33	1.61±0.43	2.28±0.73	1.45±0.40	2.08±0.93
S	S^{3+}	1.00±0.01	1.02±0.01	1.07±0.04	1.01±0.01	1.05±0.05

Table 4. Elemental abundances[a] in NGC 7635.

		C	N	O	S
K1		9.00±0.20	7.58±0.14	8.42±0.09	6.86±0.14
K2		8.77±0.14	7.47±0.12	8.49±0.06	6.96±0.08
Rim		8.59±0.18	7.23±0.15	8.33±0.06	6.77±0.09
"Whole Slit"	$t^2=0$	8.80±0.17	7.49±0.13	8.40±0.08	6.87±0.08
	$t^2>0$	8.65±0.23	7.98±0.20	8.76±0.09	7.46±0.11
Abundances expected from abundance gradients					
Shaver et al. (1983)		–	7.67±0.15	8.60±0.15	–
Afflerbach et al. (1997)		–	7.76±0.08	8.56±0.11	6.67±0.07
Deharveng et al. (2000)		–	–	8.46±0.07	–
Esteban et al. (2005)[b]		8.45±0.20	–	8.64±0.12	–
Carigi et al. (2005)[c]		–	7.74±0.20	–	–
Solar abundances					
Asplund et al. (2009)		8.43±0.05	7.83±0.05	8.69±0.05	7.12±0.03

[a] In units of $12+log(X/H)$.

[b] Determined from RLs.

[c] Determined from CELs assuming $t^2>0$.

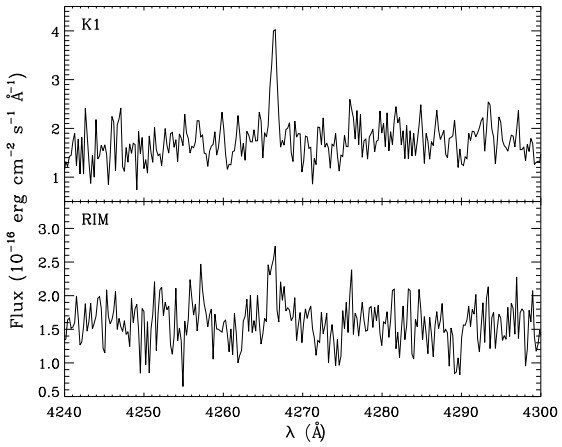

Figure 9. Sections of the integrated spectra around the emission line C II 4267 Å for the knot K1 (top panel) and the rim (botton panel) of NGC 7635.

with those of Rodríguez (1999). For the rim, our O/H ratio is somewhat lower than those of Talent & Dufour (1979) and Moore et al. (2002), both obtain a $12+log(O/H) = 8.49$. The largest differences of abundances between the knots and the rim are found for carbon. The relative contribution of C^+ –and therefore the uncertainty of the total C/H ratio– is far larger in the case of K1. One of the possible reasons of such difference may be the very different ionization degree of the knots and the rim, specially between K1 and the rim, where the O^{2+}/O^+ ratio differs in more than 1 dex (see Table 2). This strong change in the ionization degree, due to the ionization-bounded structure of the knots, involves an important variation in the ICF(C^+) (see Table 3). That fact can be affecting the suitability of the this ICF.

7 DISCUSSION

7.1 The abundance pattern of NGC 7635

Assuming the validity of the temperature fluctuation hypothesis proposed by Peimbert (1967) and that this phenomenon is related to the AD problem (see García-Rojas & Esteban 2007), we have estimated a t^2 parameter from the ADF(O^{2+}) found for the "whole slit" spectra, following the formalism outlined by Peimbert & Costero (1969) and equations (8)–(11) of Peimbert et al. (2004). The value of the t^2 parameter representative of the O^{2+} zone is 0.071±0.009. We have adopted this t^2 parameter in order to calculate the ionic abundances, the same set of ICFs (see §6) and the total abundances for the "whole slit" spectrum under the presence of temperature fluctuations. These values are also included in Tables 2, 3 and 4.

The "whole slit" abundances can be considered as the representative average values for NGC 7635 and, therefore, it seems appropriate to compare them with those expected from the Galactic abundance gradients. We have included in Table 4 the expected abundances obtained from some of the gradients determinations available in the literature, as

well as the solar values. Using the distance to NGC 7635 of 2.4±0.2 kpc adopted by Moore et al. (2002) and assuming a galactocentric distance of the Sun of 8.0±0.5 kpc (Reid 1993), we estimate a galactocentric distance of about 9.2±0.5 kpc for NGC 7635. As we can see in Table 4, the comparison of the total abundances for both possible values of t^2 and the abundance gradients is rather puzzling. Firstly, the C/H ratio obtained from the C II 4267 Å RL is larger than expected by the Galactic abundance gradient of this element derived from observations of H II regions (Esteban et al. 2005) for any of the two values of the t^2 parameter considered in the table. The difference between our C abundance determinations and the expectations of the abundance gradients is specially large in the case or the knots, but marginally consistent within the errors in the case of the rim. This could suggest that –as we outlined in Section 6– this disagreement may be due to the unsuitability of the ICF(C^+) used, at least in the case of the knots. In the case of the "whole slit" spectrum, the C^{2+}/O^{2+} ratio with respect to the excitation degree –O^{2+}/O^+ ratio– of the ionized gas is similar to the values reported for other Galactic H II regions, as S 311 (García-Rojas et al. 2005) and, therefore, the ICF(C^+) seems to be not the reason of the large C/H ratio in this particular case. The expected values of the Galactic O/H and N/H gradients are just in between our determinations for t^2=0 and t^2> 0. In particular, the O abundance expected in the abundance gradient of Esteban et al. (2005) –based on the flux of O II RLs– is marginally consistent with our determinations for t^2> 0 within the errors. Finally, the S/H ratio calculated for any value of the t^2 parameter is always larger than that expected from the S gradient of Afflerbach et al. (1997).

The lack of consistency between our abundance determinations and the Galactic abundance gradients expectations for NGC 7635 suggests that perhaps the standard methods for deriving physical conditions and chemical abundances are not giving the correct values for this object. The problem seems to affect the spectra of all selected areas: the knots, the rim and the "whole slit" ones. Firstly, the carbon abundance is too high. It is very unlikely that the nebula has suffered a pollution of C processed by the ionizing central star because it is still in the main sequence. On the other hand, due to the fact that K1 and K2 also show a very intense C II 4267 Å RL and high C^{2+}/H^+ ratios, the hypothetical chemical pollution event should also affect these structures that belong to the larger emission complex S162 (Moore et al. 2002), which is outside the bubble of NGC 7635. Another possibility of a local increase of C may be due to the destruction of carbon-rich dust by the shock associated with the expanding windblown bubble. A possibility that was already suggested by Moore et al. (2002). Esteban et al. (1998) estimated that the destruction of all the carbon locked-up onto dust grains in the Orion Nebula would increase the measured gas-phase C/H ratio in only about 0.1 dex. An increase of such magnitude would alleviate somehow the difference between the observed values and those expected by the abundance gradients, but does not account for it completely. All these problems with the flux of the C II 4267 Å RL and the high C/H ratio, specially at K1, makes us to consider that the emission flux of that line is enhanced by an unknown mechanism. We speculate that perhaps this mechanism could be related with the strong photoevaporative flow from the surfaces of the knots found by Moore et al. (2002) from *HST* images of NGC 7635. For these authors, structures as K1 are the ionized edge of a mass of neutral material associated to the S162 complex, which is ionized by the central Of-type star. The photoevaporative flow seem to be interacting with the stellar wind as it is suggested by the presence of an emission loop between the knots and the central star (Moore et al. 2002). Further deeper and higher spectral resolution spectroscopical observations of these features would be needed to shed light onto this problem.

7.2 Comparison with the Orion Nebula

The Orion Nebula is the nearest H II region and therefore the most suitable object to explore the spatial variations of the nebular properties as well as the abundance discrepancy problem at the highest spatial resolution. Mesa-Delgado et al. (2008) obtained the spatial distributions of several quantities over five slit positions in the Orion Nebula with an angular resolution set to 1.″2. They found significant small-spatial scale variations of density, temperature as well as the ADF(O^{2+}), most of them related to the presence of morphological structures such as HH objects, proplyds and ionization fronts as the Orion bar.

In this study, we have tried to obtain a similar dataset for other bright –but more distant– Galactic H II regions. However, the inventories of proplyds and HH objects in M8 and M17 are far less complete than for the Orion Nebula. Because of its different nature, there is no detection of these objects in NGC 7635. Discovering proplyds in other H II regions –apart from the Orion Nebula– is a difficult task considering their larger distances and the problems related to the discrimation between true proplyds and fragmented portions of molecular clouds (see De Marco et al. 2006). The single candidates to proplyds in M8 and M17 have been reported by Stecklum et al. (1998) –marked as UC in Fig. 1– and De Marco et al. (2006) analyzing narrow-band images taken with *HST*, respectively. On the other hand, HH objects are direct manifestations of the interaction of gas ejected by a young star with its surroundings. The existence of HH objects in M8 was firstly mentioned by Reipurth (1981), who discovered HH 213 from images with the 1-m telescope class at Las Campanas Observatory. More recently, the catalog of HH objects in M8 has increased with the spectroscopic confirmation of HH 870 (Arias et al. 2006) and the new five outflows reported by Barbá & Arias (2007) using optical narrow-band imaging with the Wide Field Imager at the 2.2-m telescope at La Silla Observatory. In the case of M17, there is not available literature about the presence of HH objects in this H II region, excluding a possible microjet found by De Marco et al. (2006).

Assuming a distance to the Orion Nebula of 436 pc (O'Dell & Henney 2008), the linear sizes of the proplyds and HH objects located at the Huygens region lie between 0.003 and 0.007 pc and 0.006 and 0.02 pc, respectively. The extractions analyzed by Mesa-Delgado et al. (2008) had an angular size of 1.″2, that corresponds to a linear resolution of 0.0025 pc. Given that resolution, Mesa-Delgado et al. (2008) could obtain enough spatial sampling to detect the spatial variations of the nebular properties associated to those morphological structures. However, the H II regions we analyse

in this paper are at larger distances than the Orion Nebula: 1.25 kpc (M8 Arias et al. 2006), 1.6 kpc (M17 Povich et al. 2007) and 2.4 kpc (NGC 7635 Moore et al. 2002). At those distances and with the size of the extractions used for each H II region in this work, the minimum linear size we can resolve is 0.0072 pc, 0.0093 pc and 0.035 pc in the case of M8, M17 and NGC 7635, respectively. As we can see, the linear resolutions that we achieve in our spatial analysis are a factor 3, 4 and 14, respectively, lower than in the case of the Orion Nebula. It is clear that spatial variations of the physical and chemical properties associated with proplyds with linear sizes similar to those of the Orion Nebula are very unlikely to be detected with our observations, except perhaps in the case of M8, where very large proplyds are of the order of our small extractions. With these comparatively large resolution elements, the emission of the proplyds –and any associated variation of the local properties of the ionized gas, if they exist– would be diluted with the emission of the ambient nebular gas. In the case of HH objects, structures similar to those observed in the Orion Nebula would be resolved with the size of the extractions used in the cases of M8 and M17. For example, knot B of HH 870 in M8 has a diameter of about 0.015 pc, similar to those found in the Orion Nebula.

If those object are present in all H II regions, we have estimated that the spatial resolution needed to resolve proplyds similar to those of the Orion Nebula should be about 0.″42 for M8, 0.″33 for M17 and 0.″22 in the case of NGC 7635, which are of the order or smaller than the best seeing attainable with ground-based telescopes.

7.3 A possible candidate to Herbig-Haro object in M8

In §5.1 we have presented several evidences that suggest the presence of a new HH object in M8. It is located approximately 16″ east and 44″ north from Her 36 and can be seen as a diffuse relatively bright arc near an ionization front (HH? in Fig. 1). This candidate to HH object presents a density 1.4 times larger than the adjacent background, somewhat lower than the density contrast found for the much prominent HH 870, which amounts to 2.3.

As we mentioned in §5.1, the HH objects typically show a strong emission of lines emitted by low ionization potential ions such as Fe^{2+}, S^{+} or O^{+}. The spatial distribution of [Fe III] 4658 Å shown in Fig. 4(c) indicates that this line is enhanced by a factor of 1.3 with respect to the surrounding background gas. This increase of the dereddened flux of [Fe III] 4658 Å is also lower than that shown by HH 870. The [S II]/Hα ratio is a good indicator to discriminate between shock-excited and photoionized gas. Arias et al. (2006) obtained a map of [S II]/Hα ratio of the central part of M8 nebula, where they reported high values of this indicator at the three nebular knots associated with HH 870. Using our data, we find that the [S II]/Hα ratio increases by a factor of 1.8 at the position of HH 870. In the case of our candidate to HH object, we have obtained an increment of about 1.3, similar to that we can estimate from the map of Arias et al. (2006). In fact the shape of the possible HH object can be well identified in the [S II] and [S II]/Hα maps of Arias et al. (2006), while it cannot be noticed in their Hα map. This behaviour is different to that we can observe in the ionization front near the candidate, which can be clearly seen in all maps. Further spectroscopic observations at higher spectral resolution would be necessary to study the kinematics of this object in order to confirm its true nature.

8 CONCLUSIONS

In this article, we have carried out long-slit spectrophotometry at intermediate spectral resolution of the Galactic H II regions M8, M17 and NGC 7635. The one-dimensional spectra were extracted with a resolution of 1.″2 for M8 and M17, and 3″ in the case of NGC 7635. Additional extractions with a spatial size of 4.″8 were necessary in order to measure the faint C II and O II RLs in M8. We have studied the spatial distributions of a large number of nebular quantities along several slit positions covering different morphological structures such as HH objects, ionization fronts or bright knots. The studied quantities were $c(\mathrm{H}\beta)$, n_e, T_e([O III]), T_e([N II]), the observed and dereddened flux of several emission lines ([Fe III] 4658 Å, C II 4267 Å, O II 4649 Å, [O III] 4959,5007 Å and [O II] 7320 Å) and the O^{2+} abundances derived from CELs and RLs, as well as the difference of both determinations, ADF(O^{2+}).

The density spatial distributions show a large range of variation across the different slit positions. We have found local maxima associated with the HG region, HH 870, knots and regions with a high surface brightness. On the other hand, the temperature spatial profiles do not show important variations related to the cited structures. The temperatures obtained from the different indicators present the classical behaviour for M8 and M17: those derived from [N II] lines are higher than those derived from [O III] lines, as expected for ionization-bounded nebulae. In the case of NGC 7635, both temperatures seem to be very similar considering the error due to the own structure of the Bubble nebula which is matter-bounded. We have also explored the spatial behaviour of the ADF(O^{2+}) along the slit positions of M8 and M17, which remains rather constant, finding values between 0.3 and 0.5 dex with an average error of about 0.1 dex.

We have analysed the physical conditions and chemical composition of four additional extractions of NGC 7635: three of them centered on the knots –K1 and K2– and the rim of the bubble; and the last one corresponding to the "whole slit" spectrum. On the one hand, the comparison of the O^{2+}/H^{+} ratio determined from CELs and RLs in the "whole slit" spectrum produces an ADF(O^{2+}) of about 0.59 dex. Assuming that the AD problem is related to temperature fluctuations, we have obtained a t^2 parameter of 0.071. We have found a puzzling pattern in the total abundances derived for NGC 7635. The total abundances obtained for the knots are slightly higher than those of the rim. The total abundances were compared with those expected by the Galactic abundance gradients, finding that there are discrepancies, specially in the case of C. We suspect that C II 4267 Å RL may be abnormally enhanced in NGC 7635 due to an unknown physical process, whose investigation is outside the scope of this paper but deserves further more detailed observations.

Comparing our observations with those of Mesa-Delgado et al. (2008), we conclude that proplyds –and the

associated variations of the local properties of the gas– with linear sizes similar to those found in the Orion Nebula cannot be resolved with the observations reported in this paper. Angular resolutions of the order or smaller than the minimun seeing reached from the ground-based telescope would be needed to distinguish the presence of proplyds.

Finally, we have found several evidences that point out to a possible new candidate to HH object in M8. This new object is located 16″ east and 44″ north from Her 36 where we have found enhancements in the spatial profile of [Fe III] 4658 Å and in [S II]/Hα map presented by Arias et al. (2006).

ACKNOWLEDGMENTS

We are vey grateful to the referee of the paper for his/her comments and suggestions. We thank J. García-Rojas, V. Luridiana and S. Simón-Díaz for their helpful suggestions. This work has been funded by the Spanish Ministerio de Ciencia y Tecnología (MCyT) under project AYA2004-07466 and Ministerio de Educación y Ciencia (MEC) under project AYA2007-63030.

REFERENCES

Afflerbach A., Churchwell E., Werner M. W., 1997, ApJ, 478, 190
Arias J. I., Barbá R. H., Maíz Apellániz J., Morrell N. I., Rubio M., 2006, MNRAS, 366, 739
Asplund M., Grevesse N., Sauval A. J., Scott P., 2009, ARA&A, 47, 481
Barbá R. H., Arias J. I., 2007, A&A, 471, 841
Blagrave K. P. M., Martin P. G., Baldwin J. A., 2006, ApJ, 644, 1006
Cardelli J. A., Clayton G. C., Mathis J. S., 1989, ApJ, 345, 245
Carigi L., Peimbert M., Esteban C., García-Rojas J., 2005, ApJ, 623, 213
Castañeda H. O., Vilchez J. M., Copetti M. V. F., 1992, A&A, 260, 370
Caulet A., 1997, Space Telesc. Eurp. Coord. Fac. Newsl., 24, 12
Christopoulou P. E., Goudis C. D., Meaburn J., Dyson J. E., Clayton C. A., 1995, A&A, 295, 509
Davey A. R., Storey P. J., Kisielius R., 2000, A&AS, 142, 85
De Marco O., O'Dell C. R., Gelfond P., Rubin R. H., Glover S. C. O., 2006, AJ, 131, 2580
Deharveng L., Peña M., Caplan J., Costero R., 2000, MNRAS, 311, 329
Ercolano B., 2009, MNRAS, 397, L69
Esteban C., 2002, in Henney W. J., Franco J., Martos M., eds, Revista Mexicana de Astronomia y Astrofisica Conference Series Vol. 12 of Revista Mexicana de Astronomia y Astrofisica Conference Series, Are Temperature Fluctuations Out There?. pp 56–61
Esteban C., Bresolin F., Peimbert M., García-Rojas J., Peimbert A., Mesa-Delgado A., 2009, ApJ, 700, 654
Esteban C., García-Rojas J., Peimbert M., Peimbert A., Ruiz M. T., Rodríguez M., Carigi L., 2005, ApJ, 618, L95
Esteban C., Peimbert M., Torres-Peimbert S., Escalante V., 1998, MNRAS, 295, 401
Esteban C., Peimbert M., Torres-Peimbert S., García-Rojas J., 1999, Rev. Mexicana Astron. Astrofis., 35, 65
Esteban C., Peimbert M., Torres-Peimbert S., García-Rojas J., Rodríguez M., 1999, ApJS, 120, 113
French H. B., 1983, ApJ, 273, 214
García-Rojas J., Esteban C., 2007, ApJ, 670, 457
García-Rojas J., Esteban C., Peimbert A., Peimbert M., Rodríguez M., Ruiz M. T., 2005, MNRAS, 362, 301
García-Rojas J., Esteban C., Peimbert A., Rodríguez M., Peimbert M., Ruiz M. T., 2007, Revista Mexicana de Astronomia y Astrofisica, 43, 3
Garnett D. R., Shields G. A., Peimbert M., Torres-Peimbert S., Skillman E. D., Dufour R. J., Terlevich E., Terlevich R. J., 1999, ApJ, 513, 168
Hanson M. M., Conti P. S., 1995, ApJ, 448, L45
Harrington J. P., Feibelman W. A., 1984, ApJ, 277, 716
Kingdon J., Ferland G. J., 1995, ApJ, 442, 714
Liu X.-W., Barlow M. J., Zhang Y., Bastin R. J., Storey P. J., 2006, MNRAS, 368, 1959
Liu X.-W., Storey P. J., Barlow M. J., Danziger I. J., Cohen M., Bryce M., 2000, MNRAS, 312, 585
Martín-Hernández N. L., Esteban C., Mesa-Delgado A., Bik A., Puga E., 2008, A&A, 482, 215
Mathis J. S., Liu X.-W., 1999, ApJ, 521, 212
Mendoza C., 1983, in Flower D. R., ed., Planetary Nebulae Vol. 103 of IAU Symposium, Recent advances in atomic calculations and experiments of interest in the study of planetary nebulae. pp 143–172
Mesa-Delgado A., Esteban C., García-Rojas J., 2008, ApJ, 675, 389
Mesa-Delgado A., Esteban C., García-Rojas J., Luridiana V., Bautista M., Rodríguez M., López-Martín L., Peimbert M., 2009, MNRAS, 395, 855
Mesa-Delgado A., López-Martín L., Esteban C., García-Rojas J., Luridiana V., 2009, MNRAS, 394, 693
Moore B. D., Walter D. K., Hester J. J., Scowen P. A., Dufour R. J., Buckalew B. A., 2002, AJ, 124, 3313
O'Dell C. R., Henney W. J., 2008, AJ, 136, 1566
Osterbrock D. E., Ferland G. J., 2006, Astrophysics of gaseous nebulae and active galactic nuclei. 2nd. ed. Sausalito, CA: University Science Books
Peimbert A., Peimbert M., 2005, in Torres-Peimbert D., MacAlpine G., eds, Rev. Mexicana Astron. Astrofis. Conf. Ser. Vol. 23, Oxygen Recombination Line Abundances in Gaseous Nebulae. p. 9
Peimbert M., 1967, ApJ, 150, 825
Peimbert M., Costero R., 1969, Boletin de los Observatorios Tonantzintla y Tacubaya, 5, 3
Peimbert M., Peimbert A., 2006, in Barlow M. J., Méndez R. H., eds, Planetary Nebulae in our Galaxy and Beyond Vol. 234 of IAU Symposium, Temperature Variations and Chemical Abundances in Planetary Nebulae. pp 227–234
Peimbert M., Peimbert A., Ruiz M. T., Esteban C., 2004, ApJS, 150, 431
Peimbert M., Storey P. J., Torres-Peimbert S., 1993, ApJ, 414, 626
Peimbert M., Torres-Peimbert S., Dufour R. J., 1993, ApJ, 418, 760
Peimbert M., Torres-Peimbert S., Ruiz M. T., 1992, Rev. Mexicana Astron. Astrofis., 24, 155

Povich M. S., Stone J. M., Churchwell E., Zweibel E. G., Wolfire M. G., Babler B. L., Indebetouw R., Meade M. R., Whitney B. A., 2007, ApJ, 660, 346
Reid M. J., 1993, ARA&A, 31, 345
Reipurth B., 1981, A&AS, 44, 379
Rodríguez M., 1999, A&A, 351, 1075
Rodríguez M., García-Rojas J., 2010, ApJ, 708, 1551
Rola C., Stasinska G., 1994, A&A, 282, 199
Rubin R. H., 1969, ApJ, 155, 841
Sánchez L. J., Peimbert M., 1991, Rev. Mexicana Astron. Astrofis., 22, 285
Shaver P. A., McGee R. X., Newton L. M., Danks A. C., Pottasch S. R., 1983, MNRAS, 204, 53
Shaw R. A., Dufour R. J., 1995, PASP, 107, 896
Stasińska G., 1978, A&A, 66, 257
Stasińska G., 1980, A&A, 85, 359
Stasińska G., Tenorio-Tagle G., Rodríguez M., Henney W. J., 2007, A&A, 471, 193
Stecklum B., Henning T., Feldt M., Hayward T. L., Hoare M. G., Hofner P., Richter S., 1998, AJ, 115, 767
Storey P. J., 1994, A&A, 282, 999
Storey P. J., Hummer D. G., 1995, MNRAS, 272, 41
Talent D. L., Dufour R. J., 1979, ApJ, 233, 888
Tenorio-Tagle G., 1996, AJ, 111, 1641
Tsamis Y. G., Barlow M. J., Liu X.-W., Danziger I. J., Storey P. J., 2003, MNRAS, 338, 687
Tsamis Y. G., Barlow M. J., Liu X.-W., Storey P. J., Danziger I. J., 2004, MNRAS, 353, 953
Tsamis Y. G., Péquignot D., 2005, MNRAS, 364, 687
Tsamis Y. G., Walsh J. R., Péquignot D., Barlow M. J., Danziger I. J., Liu X.-W., 2008, MNRAS, 386, 22
Woodward C. E., Pipher J. L., Helfer H. L., Sharpless S., Moneti A., Kozikowski D., Oliveri M., Willner S. P., Lacasse M. G., Herter T., 1986, AJ, 91, 870

APPENDIX A: EMISSION LINE FLUXES

In Table A1, we present the aperture number (Column 1), Hβ observed fluxes in units of erg cm^2 s^{-1} (Column 2), dereddened flux line ratios of the main emission lines (Columns 3-14) per slit position in untis of $I(\mathrm{H}\beta) = 100$ and the average extinction coeficient (last row of each slit position). Several notes should be considered in order to understand Table A1:

(*i*) The aperture number (Ap) is the identification number of each one-dimensional spectra extracted and it is related to the positional measurement in arcseconds as $\mathrm{Ap}_{initial}+\mathrm{Ap}_{size}\times\mathrm{Ap}$. $\mathrm{Ap}_{initial}$ corresponds to the position in arcseconds after the edges of the CCD were discarded for the extraction of one-dimensional spectra (see extraction procedure in §3). $\mathrm{Ap}_{initial}$ amounts to 34″ in M8 POS1 and POS2, 10″ in M17 and 82″ in NGC 7635. Ap_{size} is the extraction size in arcseconds along the spatial direction (see the selected sizes in §3).
(*ii*) In order to interpret correctly the Ap column in M8 POS2 we should consider that apertures 65, 66, 67 and 68 were removed in this position due to contamination by stellar emission (see §3).
(*iii*) We have not included the errors associated with Hβ observed fluxes which remain between 3% and 5% among the different slit positions.
(*iv*) We have only listed [O III] 4959 Å and [N II] 6548 Å nebular lines. [O III] 5007 Å and [N II] 6583 Å can be obtained from the first ones using their theoretical relation:

$$I([\mathrm{O\ III}]\ 5007)/I([\mathrm{O\ III}]\ 4959) = 2.88 \qquad \text{(A1)}$$

and

$$I([\mathrm{N\ II}]\ 6583)/I([\mathrm{N\ II}]\ 6548) = 2.92. \qquad \text{(A2)}$$

(*v*) In the cases of M8 POS1 and POS2, it should be reminded that additional extractions of 4.″8 wide were obtained to achieve proper flux measurements of O II RLs (see §3). In this sense, an aperture of 4.″8 wide represents the average value of four apertures extracted with an angular size of 1.″2. The vertical lines in the left-hand side of the O II RLs cover the four apertures of 1.″2 wide.